Weak-light rogue waves, breathers, and their active control in a cold atomic gas via electromagnetically induced transparency

Junyang Liu,[1] Chao Hang,[1,2,*] and Guoxiang Huang[1,2,†]

[1]*State Key Laboratory of Precision Spectroscopy, School of Physical and Material Sciences, East China Normal University, Shanghai 200062, China*

[2]*NYU-ECNU Joint Institute of Physics at NY-Shanghai, Shanghai 200062, China*

(Received 7 March 2016; published 21 June 2016)

We propose a scheme to demonstrate the existence of optical Peregrine rogue waves and Akhmediev and Kuznetsov-Ma breathers and realize their active control via electromagnetically induced transparency (EIT). The system we suggest is a cold, Λ-type three-level atomic gas interacting with a probe and a control laser fields and working under EIT condition. We show that, based on EIT with an incoherent optical pumping, which can be used to cancel optical absorption, (1+1)-dimensional optical Peregrine rogue waves, Akhmediev breathers, and Kuznetsov-Ma breathers can be generated with very low light power. In addition, we demonstrate that the Akhmediev and Kuznetsov-Ma breathers in (2+1)-dimensions obtained can be actively manipulated by using an external magnetic field. As a result, these breathers can display trajectory deflections and bypass obstacles during propagation.

DOI: 10.1103/PhysRevA.93.063836

I. INTRODUCTION

Rogue waves are rare, strong wave packets that may appear in oceans when special conditions are met [1,2]. In recent years, they have been discovered in different physical systems, including optical fibers and cavities [3–6], water waves [7], plasma with negative ions [8], laser filamentation [9], Bose-Einstein condensates [10], whispering-gallery-mode resonators [11], photorefractive crystals [12], nd so on. On the other hand, they have been studied in different mathematical models, including the standard nonlinear Schrödinger (NLS) equation [13], generalized NLS equation with variable coefficients [14], derivative NLS equation [15], Hirota equation [16–18], Davey-Stewartson equations [19], and so on.

The formation of a rogue wave is due to the amplification of a wide range of initial frequency components by modulation instability, and hence the resulting wave can reach amplitude substantially higher than that given by initial conditions [20]. In particular, zero-frequency perturbation leads to a wave packet with the highest amplitude, which is known as a Peregrine rogue wave [21]. The Peregrine rogue wave belongs to a limiting case of the one-parameter family of Kuznetsov-Ma breathers (KMB) [22] and also of one-parameter family of Akhmediev breathers (AB) [23], which is localized in two dimensions and described by rational expression. Recent studies have shown that even higher amplitudes can be reached due to the wave packets that are described by higher-order rational solutions [24]. In addition, the high-dimensional [25] and the vector properties [26] of rogue waves have also been investigated.

Among various rogue waves, optical rogue waves have attracted a great deal of interest [27,28] because of their potential applications, such as supercontinuum generation [29] and photolithography [30]. The generation of optical rogue waves, however, is very difficult in conventional optical media because the nonlinearity in those media such as optical fibers and waveguides is very weak, and hence large input power or very short pulse duration is needed in order to bring out the nonlinear effect required for the rogue wave formation [3–5]. Although the nonlinear effect can be enhanced by the use of some resonant mechanisms, there is, however, a significant optical absorption, which leads to serious attenuation and distortion of optical pulses.

In this work, we propose a scheme to demonstrate the existence of optical Peregrine rogue waves and Akhmediev and Kuznetsov-Ma breathers and realize their active control via electromagnetically induced transparency (EIT). EIT is a remarkable quantum interference effect typically occurring in multilevel atomic systems, by which light absorption due to the resonance between light field and atoms can be largely eliminated [31]. The system we suggest is a cold, Λ-type three-level atomic gas interacting with a probe and a control laser fields and working under EIT condition. Based on Maxwell-Bloch (MB) equations, we derive a nonlinear envelope equation governing the evolution of probe-field envelope. We first show that, based on EIT with an incoherent optical pumping which can be used to cancel optical absorption, (1+1)-dimensional [(1+1)D] optical Peregrine rogue waves and Akhmediev and Kuznetsov-Ma breathers can be generated at very low light power. Furthermore, we discuss the initial condition necessary for the creation of Peregrine rogue waves. In addition, we demonstrate that the Akhmediev and Kuznetsov-Ma breathers in (2+1)D obtained in our system can be actively manipulated by using an external magnetic field. As a result, these breathers can display trajectory deflections and bypass obstacles during their propagation. Our work opens an avenue for the study of optical rogue waves and breathers in resonant optical media and realize their active manipulations at very low light level.

The article is arranged as follows. In Sec. II, the physical model under study is described. In Sec. III, the nonlinear equation governing the evolution of the probe-field envelope is derived. In Sec. IV, the Peregrine rogue waves, Akhmediev breathers, and Kuznetsov-Ma breathers are obtained, and

*chang@phy.ecnu.edu.cn
†gxhuang@phy.ecnu.edu.cn

their generation powers are estimated. In Sec. V, the active control of Akhmediev and Kuznetsov-Ma breathers by using an external magnetic field is investigated. Finally, the last section (Sec. VI) summarizes the main results obtained in this work.

II. MODEL

We start with considering a lifetime-broadened atomic gas with a Λ-type three-level configuration, interacting with a weak, pulsed probe field (with the time duration τ_0 and beam radius $R_\perp$ at the entrance of the medium) of center angular frequency ω_p that drives the transition $|1\rangle \leftrightarrow |3\rangle$ and a strong, continuous-wave control field of center angular frequency ω_c that drives the transition $|2\rangle \leftrightarrow |3\rangle$, respectively; see Fig. 1(a). The electric-field vector of the system can be written as $\mathbf{E} = \mathbf{E}_p + \mathbf{E}_c = \sum_{l=c,p} \mathbf{e}_l \mathcal{E}_l \exp[i(\mathbf{k}_l \cdot \mathbf{r} - \omega_l t)] + \text{c.c.}$, where $\mathbf{e}_p$ and $\mathcal{E}_p$ ($\mathbf{e}_c$ and $\mathcal{E}_c$) are, respectively, the polarization unit vector and the envelope of the probe (control) field; $k_p = \omega_p/c$ ($k_c = \omega_c/c$) is the wave number of the probe (control) field before entering into the atomic gas, and c.c. means complex conjugate. The atoms are trapped in a gas cell and initially prepared in the ground-state level $|1\rangle$. To cancel atomic collisions and Doppler effect, we assume the atoms have been cooled into a very low temperature (say, around 1 mK [32]), and both the probe and the control fields are arranged to propagate along the z direction.

Using electric-dipole and rotating-wave approximations, the Hamiltonian of the system in the interaction picture reads $H_{\text{int}}/\hbar = \sum_{j=2}^{3} \Delta_j |j\rangle\langle j| + \Omega_p |3\rangle\langle 1| + \Omega_c |3\rangle\langle 2| + \text{H.c.}$. Here $\Omega_p = (\mathbf{e}_p \cdot \mathbf{p}_{31})\mathcal{E}_p/\hbar$ and $\Omega_c = (\mathbf{e}_c \cdot \mathbf{p}_{32})\mathcal{E}_c/\hbar$ are respectively the Rabi frequencies of the probe and control fields, with $\mathbf{p}_{jl}$ being the electric dipole matrix element associated with the transition from states $|l\rangle$ to $|j\rangle$; $\Delta_2 = (\omega_p - \omega_c - \omega_{21})$ and $\Delta_3 = (\omega_p - \omega_{31})$ are, respectively, the two- and one-photon detunings, with $\omega_{jl} = (E_j - E_l)/\hbar$ (E_j is the eigenenergy of the state $|j\rangle$). The atomic motion of the system is described by the optical Bloch equations [33]

$$i\frac{\partial}{\partial t}\sigma_{11} + i\Gamma_{31}\sigma_{11} - i\Gamma_{13}\sigma_{33} + \Omega_p^*\sigma_{31} - \Omega_p\sigma_{31}^* = 0, \quad (1a)$$

$$i\frac{\partial}{\partial t}\sigma_{22} - i\Gamma_{23}\sigma_{33} + \Omega_c^*\sigma_{32} - \Omega_c\sigma_{32}^* = 0, \quad (1b)$$

$$i\frac{\partial}{\partial t}\sigma_{33} - i\Gamma_{31}\sigma_{11} + i\Gamma_3\sigma_{33} - \Omega_p^*\sigma_{31} + \Omega_p\sigma_{31}^* - \Omega_c^*\sigma_{32} + \Omega_c\sigma_{32}^* = 0, \quad (1c)$$

$$\left(i\frac{\partial}{\partial t} + d_{21}\right)\sigma_{21} - \Omega_p\sigma_{32}^* + \Omega_c^*\sigma_{31} = 0, \quad (1d)$$

$$\left(i\frac{\partial}{\partial t} + d_{31}\right)\sigma_{31} - \Omega_p(\sigma_{33} - \sigma_{11}) + \Omega_c\sigma_{21} = 0, \quad (1e)$$

$$\left(i\frac{\partial}{\partial t} + d_{32}\right)\sigma_{32} - \Omega_c(\sigma_{33} - \sigma_{22}) + \Omega_p\sigma_{21}^* = 0, \quad (1f)$$

where σ_{jl} ($j,l = 1,2,3$) are density matrix elements in the interaction picture, $d_{21} = \Delta_2 + i\gamma_{21}$, $d_{31} = \Delta_3 + i\gamma_{31}$, and $d_{32} = (\Delta_3 - \Delta_2) + i\gamma_{32}$. The composite decay rate γ_{jl} is given by $\gamma_{jl} = (\Gamma_j + \Gamma_l)/2 + \gamma_{jl}^{\text{col}}$. Here $\Gamma_j = \sum_{j<l} \Gamma_{jl}$, with Γ_{jl} being the spontaneous emission decay rate from $|l\rangle$ to $|j\rangle$ and γ_{jl}^{col} being the dephasing rate reflecting the loss of phase coherence between $|j\rangle$ and $|l\rangle$ without changing of population [33]. For the aim of introducing a gain into the system, an incoherent optical pumping, which can pump atoms from the ground-state level $|1\rangle$ to the excited-state level $|3\rangle$ with the pumping rate Γ_{31}, is introduced. The presence of the incoherent optical pumping is crucial for the existence of rogue waves, as shown below.

The equation of motion for Ω_p can be obtained by Maxwell equation, which, under the slowly varying envelope approximation, reads [34]

$$i\left(\frac{\partial}{\partial z} + \frac{1}{c}\frac{\partial}{\partial t}\right)\Omega_p + \frac{c}{2\omega_p}\frac{\partial^2\Omega_p}{\partial x^2} + \kappa_{13}\sigma_{31} = 0. \quad (2)$$

Here $\kappa_{13} = N_a\omega_p|\mathbf{p}_{13}|^2/(2\varepsilon_0 c\hbar)$, with N_a being atomic density. Note that, for simplicity, we have assumed that the probe pulse has a large spatial width in y direction so the diffraction effect in the y direction (i.e., $\partial^2\Omega_p/\partial y^2$) can be neglected.

The above model can be easily realized in realistic physical systems. One of these candidates is a cold ^{85}Rb atomic gas with energy levels assigned as $|1\rangle = |5\,^2S_{1/2}, F = 2, m_F = 0\rangle$ ($g_F = -1/3$), $|2\rangle = |5\,^2S_{1/2}, F = 3, m_F = 2\rangle$ ($g_F = 1/3$), and $|3\rangle = |5\,^2P_{1/2}, F = 3, m_F = 1\rangle$ ($g_F = 1/9$). Then the probe field is σ^+ polarized while the control field is σ^- polarized. The decay rates are given by $\Gamma_{13} \approx \Gamma_{23} \approx \pi \times 5.75$ MHz, $\gamma_{13}^{\text{col}} \approx \gamma_{23}^{\text{col}} \approx 1$ kHz, and $|\mathbf{p}_{13}| = 2.54 \times 10^{-27}$ C cm [35]. The atomic density is taken as $N_a \approx 3.67 \times 10^{10}\text{cm}^{-3}$, and hence κ_{13} takes the value of $1.0 \times 10^9\ \text{cm}^{-1}\text{s}^{-1}$. All calculations given below will be based on this set of system parameters.

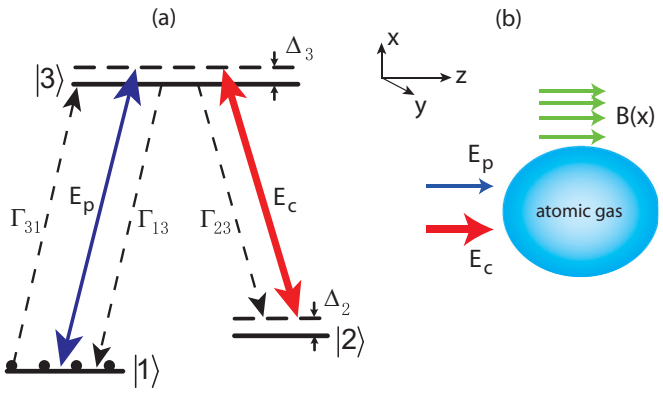

FIG. 1. (a) Energy-level diagram and excitation scheme of Λ-type three-level atoms interacting with a weak, pulsed probe field E_p and a strong, continuous-wave control field E_c. Δ_2 and Δ_3 are the two- and one-photon detunings, respectively. Γ_{13} (Γ_{23}) is the decay rate from $|3\rangle$ to $|1\rangle$ ($|3\rangle$ to $|2\rangle$). Γ_{31} is the incoherent pumping rate from $|1\rangle$ to $|3\rangle$. The atoms are initially populated in the ground state $|1\rangle$ (indicated by black dots). (b) The coordinate frame and geometrical arrangement of the system. $B(x)$ is the space-dependent gradient magnetic field applied to the atomic gas used to make an active control of the probe field.

III. ASYMPTOTIC EXPANSION AND NONLINEAR ENVELOPE EQUATION

One of the main goals of the present work is to obtain rogue waves and breathers in the system described above. To this end, we first derive the envelope equation of the probe field based on the MB Eqs. (1) and (2) by using the standard method of multiple scales [36]. Taking the asymptotic expansion $\sigma_{jk} = \delta_{j1}\delta_{k1} + \epsilon\sigma_{jk}^{(1)} + \epsilon^2\sigma_{jk}^{(2)} + \epsilon^3\sigma_{jk}^{(3)}$ $(j,k = 1,2,3$; both δ_{j1} and δ_{k1} are Kronecker δ symbols), $\Omega_p = \epsilon\Omega_p^{(1)} + \epsilon^2\Omega_p^{(2)} + \epsilon^3\Omega_p^{(3)}$, and $d_{jk} = d_{jk}^{(0)} + \epsilon d_{jk}^{(1)} + \epsilon^2 d_{jk}^{(2)} + \epsilon^3 d_{jk}^{(3)}$ $(j,k = 1,2,3; j \neq k)$. Here ϵ is a small parameter characterizing the small population depletion of the ground state, and all quantities on the right-hand side of the asymptotic expansion are considered as functions of the multiscale variables $z_l = \epsilon^l z$ $(l = 0,1,2)$, $x_1 = \epsilon x$, and $t_l = \epsilon^l t$ $(l = 0,1)$. Thus, we have $d_{21}^{(0)} = (\omega_p - \omega_c - \omega_{21}) + i\gamma_{21}$, $d_{31}^{(0)} = (\omega_p - \omega_{31}) + i\gamma_{31}$, $d_{32}^{(0)} = (\omega_c - \omega_{32}) + i\gamma_{32}$, and $d_{21}^{(j)} = d_{31}^{(j)} = d_{32}^{(j)} = 0$ $(j = 1,2,3)$. Substituting these expansions into the MB Eqs. (1) and (2), and comparing the coefficients of ϵ^l $(l = 1,2,3\cdots)$, we obtain a set of linear but inhomogeneous equations which can be solved order by order.

The solution at the zero (leading) order $(l = 0)$ reads

$$\sigma_{11}^{(0)} = \frac{|\Omega_c|^2 X}{i\Gamma_{23}\Gamma_{31}/\Gamma_{13} + |\Omega_c|^2(2\Gamma_{31}/\Gamma_{13} + 1)X}, \qquad (3)$$

$\sigma_{33}^{(0)} = (\Gamma_{31}/\Gamma_{13})\sigma_{11}^{(0)}$, $\sigma_{22}^{(0)} = 1 - \sigma_{11}^{(0)} - \sigma_{33}^{(0)}$, $\sigma_{21}^{(0)} = \sigma_{31}^{(0)} = 0$, and $\sigma_{32}^{(0)} = \Omega_c(\sigma_{33}^{(0)} - \sigma_{22}^{(0)})/d_{32}^{(0)}$, with $X = 1/d_{32}^{(0)*} - 1/d_{32}^{(0)}$. Notice that when the incoherent pumping $\Gamma_{31} = 0$, we have $\sigma_{11}^{(0)} = 1$ and $\sigma_{22}^{(0)} = \sigma_{33}^{(0)} = \sigma_{32}^{(0)} = \sigma_{21}^{(0)} = \sigma_{31}^{(0)} = 0$.

At the first order $(l = 1)$, we obtain the solution $\Omega_p^{(1)} = Fe^{i\theta}$, $\sigma_{31}^{(1)} = a_{31}^{(1)}Fe^{i\theta}$, and $\sigma_{21}^{(1)} = a_{21}^{(1)}F\,e^{i\theta}$, with $\theta = K(\omega)z_0 - \omega t_0$ [37], F being a yet-to-be-determined envelope function of the slow variables t_1, x_1, and z_2, and the expressions of $a_{j1}^{(1)}(j = 2,3)$ given in Appendix. The linear dispersion relation of the system is given by

$$K(\omega) = \frac{\omega}{c} + \kappa_{13}\frac{\Omega_c\sigma_{32}^{(0)*} + (\omega + d_{21}^{(0)})(\sigma_{11}^{(0)} - \sigma_{33}^{(0)})}{D(\omega)}, \qquad (4)$$

where we have defined $D(\omega) = |\Omega_c|^2 - (\omega + d_{21}^{(0)})(\omega + d_{31}^{(0)})$.

Shown in Fig. 2 is the imaginary part of K, i.e., $\mathrm{Im}(K)$, as a function of ω, characterizing the absorption in the system. The red thin solid line in the figure is for $(\Omega_c,\Gamma_{31}) = (0,0)$, which indicates that in the absence of the control field and the incoherent pumping the probe field has a very large absorption near $\omega = 0$ (corresponding to the center frequency of the probe field); however, when Ω_c takes the value of 5×10^7 Hz and the incoherent pumping is still absent, a transparency window in the profile of $\mathrm{Im}(K)$ is opened, as shown by the green thick solid line. This is the well-known EIT phenomenon induced by the quantum interference effect contributed by the control field. However, in this case there is still a small residual absorption $[\mathrm{Im}(K) \approx 0.2]$ around $\omega = 0$; see the insert of the figure. That is to say, although the EIT can suppress the absorption largely, it cannot make the absorption to be exact zero. This small residual absorption is caused from the small

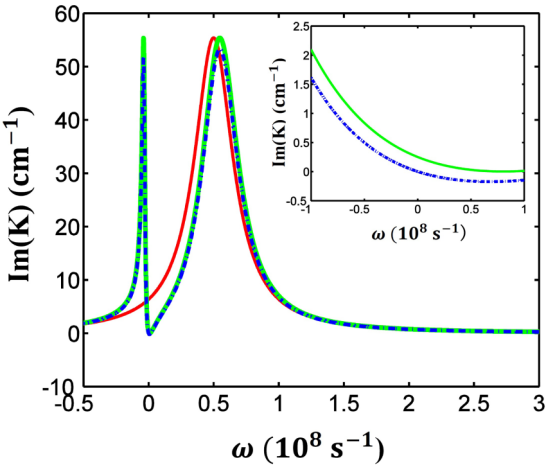

FIG. 2. $\mathrm{Im}(K)$ versus ω for $(\Omega_c,\Gamma_{31}) = (0,0)$ (red thin solid line), $(1.6 \times 10^7, 0)$ (green thick solid line), and $(1.6 \times 10^7, 9.1 \times 10^4)$ (blue dashed-dotted line). The insert shows respectively the curves for $(\Omega_c,\Gamma_{31}) = (1.6 \times 10^7, 0)$ and $(1.6 \times 10^7, 9.1 \times 10^4)$ around $\omega = 0$, which indicates that the system has a gain for nonzero Γ_{31} (incoherent pumping).

decay rate (γ_{21}) between the two lower states $|1\rangle$ and $|2\rangle$. The blue dashed-dotted line in Fig. 2 represents the situation when the incoherent pumping Γ_{31} takes the value of 9.1×10^4 s^{-1}. One can see that in this case the absorption is nearly vanishing $[\mathrm{Im}(K) \approx 0]$ near $\omega = 0$. This is because the incoherent pumping contributes a gain, which cancels the absorption of the system. The presence of the incoherent pumping is crucial to the existence of rogue waves and breathers because even a small absorption will lead to a serious attenuation in rogue waves and breathers; see Fig. 4 below.

At the second order $(l = 2)$, a divergence-free condition requires

$$i\left(\frac{\partial F}{\partial z_1} + \frac{1}{V_g}\frac{\partial F}{\partial t_1}\right) = 0, \qquad (5)$$

where $V_g = 1/K_1 = (\partial K/\partial\omega)^{-1}$ is group velocity of the envelope function F. The solution at the second order reads $\sigma_{j1}^{(2)} = a_{j1}^{(2)}(\partial F/\partial t_1)e^{i\theta}(j = 2,3)$, $\sigma_{jj}^{(2)} = a_{jj}^{(2)}|F|^2e^{-\alpha z_2}(j = 1,2)$, and $\sigma_{33}^{(2)} = -\sigma_{11}^{(2)} - \sigma_{22}^{(2)}$, with the expressions of $a_{j1}^{(2)}(j = 2,3)$ and $a_{jj}^{(2)}(j = 1,2)$ given in Appendix.

With the above solution, we go to the third order $(l = 3)$. To get a divergence-free solution at this order, the envelope function F must satisfy the nonlinear equation

$$i\frac{\partial F}{\partial z_2} - \frac{1}{2}K_2\frac{\partial^2 F}{\partial t_1^2} + \frac{c}{2\omega_p}\frac{\partial^2 F}{\partial x_1^2} + W|F|^2Fe^{-2\alpha z_2} = 0, \qquad (6)$$

with $\alpha = \epsilon^{-2}\mathrm{Im}[K(\omega)]$, and

$$W = \kappa_{13}\frac{\Omega_c a_{32}^{(2)*} + (\omega + d_{21}^{(0)})(2a_{11}^{(2)} + a_{22}^{(2)})}{D}.$$

Here $K_2 = \partial^2 K(\omega)/\partial\omega^2$ characterizes the group velocity dispersion while W characterizes the Kerr nonlinear effect of the system.

Combing Eqs. (5) and (6) and returning to the original variables, we obtain

$$i\left(\frac{\partial}{\partial z}+\alpha\right)U-\frac{1}{2}K_2\frac{\partial^2 U}{\partial\tau^2}+\frac{c}{2\omega_p}\frac{\partial^2 U}{\partial x^2}+W|U|^2U=0, \quad (7)$$

where $\tau=t-z/V_g$ and $U=\epsilon F e^{-\alpha z}$. Equation (7) can be further written into the dimensionless form

$$i\frac{\partial u}{\partial s}+\frac{1}{2}\left(d_{\rm Dis}\frac{\partial^2}{\partial\sigma^2}+d_{\rm Dif}\frac{\partial^2}{\partial\xi^2}\right)u+|u|^2u=-id_Au, \quad (8)$$

where $s=z/L_{\rm Non}$, $\sigma=\tau/\tau_0$, $\xi=x/R_\perp$, and $u=U/U_0$ (U_0 is the characteristic Rabi frequency of the probe field). Here $L_{\rm Non}=1/(U_0^2|\tilde{W}|)$ is the characteristic nonlinearity length characterizing Kerr effect (here and in the following, the quantity with a tilde above means its real part). The dimensionless coefficients are given by $d_{\rm Dis}=L_{\rm Non}/L_{\rm Dis}$, $d_{\rm Dif}=L_{\rm Non}/L_{\rm Dif}$ and $d_A=L_{\rm Non}/L_A$, with $L_{\rm Dis}=\tau_0^2/|\tilde{K}_2|$ the characteristic dispersion length, $L_{\rm Dif}=\omega_pR_\perp^2/c$ the characteristic diffraction length, and $L_A=1/\alpha$ the characteristic absorption length of the system.

When obtaining Eq. (8) the imaginary part of the coefficients have been neglected. This is reasonable because under the EIT condition the imaginary parts can be made much smaller than their real parts (see the example given below). In addition, the coefficient d_A is very small, and hence the linear absorption term on the right-hand side of Eq. (8) can be treated as a small perturbation.

IV. WEAK-LIGHT ROGUE WAVES AND BREATHERS IN (1+1)D

A. Peregrine rogue waves in (1+1)D

Equation (8) in the absence of linear absorption (i.e., $d_A=0$), which can be realized by choosing a nonzero incoherent optical pumping Γ_{31}, has the form of a (2+1)D NLS equation. In order to obtain analytical solutions, one can employ additional condition so it can be reduced to a (1+1)D model. To be specific, we first consider the situation $d_{\rm Dis}=1$ and $d_{\rm Dif}\ll 1$, which can be achieved by taking $L_{\rm Dis}=L_{\rm Non}$ and $L_{\rm Dif}\gg L_{\rm Non}$, i.e., the dispersion and nonlinearity balance each other while the diffraction is insignificant, corresponding to the conditions $\tau_0=(|\tilde{K}_2|/|\tilde{W}|)^{1/2}U_0^{-1}$ and $R_\perp\gg[c/(\omega_p|\tilde{W}|)]^{1/2}U_0^{-1}$, respectively. In this case Eq. (8) reduces to the standard (1+1)D NLS equation

$$i\frac{\partial u}{\partial s}+\frac{1}{2}\frac{\partial^2 u}{\partial\sigma^2}+|u|^2u=0. \quad (9)$$

As an example, we take a set of system parameters given as $\Omega_c=1.6\times10^7\ {\rm s}^{-1}$, $\Delta_2=-8.0\times10^5\ {\rm s}^{-1}$, $\Delta_3=-5.0\times10^7{\rm s}^{-1}$, $\tau_0=4.0\times10^{-6}$ s, $R_\perp=0.05$ cm, $U_0=2.2\times10^6\ {\rm s}^{-1}$, and $\Gamma_{31}=9.1\times10^4\ {\rm s}^{-1}$. Then we have $K_0\approx(-2.99+i0.01)\ {\rm cm}^{-1}$, $K_1\approx(5.11-i0.59)\times10^{-6}{\rm cm}^{-1}$ s, $K_2\approx(-2.24+i1.28)\times10^{-12}{\rm cm}^{-1}\ {\rm s}^2$, and $W\approx(2.86-i0.09)\times10^{-14}\ {\rm cm}^{-1}\ {\rm s}^2$ (all values are obtained at $\omega=0$). It is obvious that the imaginary parts of K_j ($j=0,1,2$) and W are much smaller than their corresponding real parts, as indicated at the end of the last section. Based on these results, we obtain the characteristic lengths of the system, given by $L_{\rm Dis}=L_{\rm Non}\approx7.1$ cm, $L_{\rm Dif}=200$ cm, and $L_A\approx193$ cm. Then we have $d_A\approx0$, $d_{\rm Dis}=1$, and $d_{\rm Dif}\approx0$. After neglecting the terms proportional to d_A and $d_{\rm Dif}$, Eq. (9) admits the first-order Peregrine soliton solution (rogue wave), having the rational form $u(s,\sigma)=[1-4(1+2is)/(1+4s^2+4\sigma^2)]e^{is}$, which is an algebraically decaying wave packet in the z direction and time, with the maximum intensity $|u|^2_{\rm max}=9$ located at $(s,\sigma)=(0,0)$. Notice that such a maximum intensity is much larger than that of the continuous-wave solution and hyperbolic secant soliton solution. After returning to the original variables, we obtain

$$\Omega_p(z,t)=U_0\left(1-4\frac{1+2iz/L_{\rm Non}}{1+4z^2/L_{\rm Non}^2+4[(t-z/\tilde{V}_g)/\tau_0]^2}\right)\times e^{iz/L_{\rm Non}}, \quad (10)$$

i.e., the probe-field envelope is localized (with the maximum $|\Omega_p|^2_{\rm max}=9U_0^2$) and travels with velocity $\tilde{V}_g$, which is estimated as

$$\tilde{V}_g\approx6.44\times10^{-6}c. \quad (11)$$

Hence the traveling velocity of the Peregrine rogue wave is very slow comparing with c (the light speed in vacuum) due to the EIT effect.

The initial condition for producing the rogue wave solution (10) can be taken as $u_i=\rho_ie^{i\theta_i}$, with

$$\rho_i^2=1+\frac{8\left(1+4z_i^2/L_{\rm Non}^2-4\tau_i^2/\tau_0^2\right)}{\left(1+4z_i^2/L_{\rm Non}^2+4\tau_i^2/\tau_0^2\right)^2}, \quad (12a)$$

$$\theta_i=\frac{z_i}{L_{\rm Non}}-\frac{2z_i/L_{\rm Non}}{z_i^2/L_{\rm Non}^2+\tau_i^2/\tau_0^2-3/4}, \quad (12b)$$

with $\tau_i=t_i-z_i/\tilde{V}_g$. Solving Eq. (9) together with the above initial condition we can obtain the propagation profile of the probe-field intensity. Shown in Fig. 3(a) is the

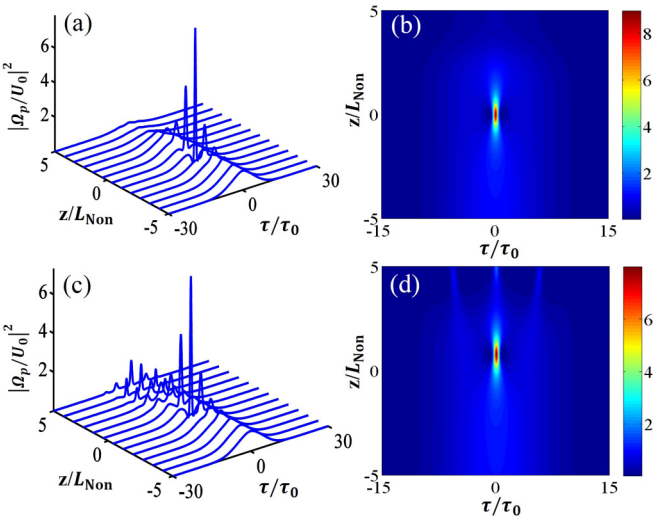

FIG. 3. (a) Probe-field intensity $|\Omega_p/U_0|^2$ versus τ/τ_0 (with $\tau=t-z/\tilde{V}_g$) and $z/L_{\rm Non}$ obtained by using the initial condition (12), with (b) the corresponding contour map; (c) $|\Omega_p/U_0|^2$ obtained by using the pure phase-engineering initial condition, with (d) the corresponding contour map.

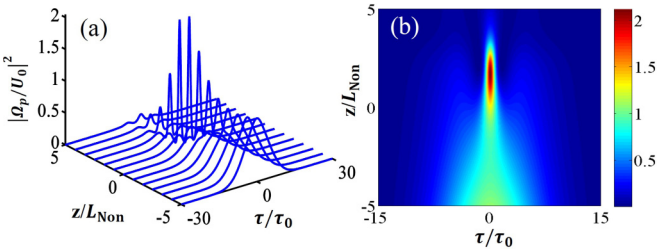

FIG. 4. (a) The probe-field intensity $|\Omega_p/U_0|^2$ versus τ/τ_0 (with $\tau = t - z/\tilde{V}_g$) and $z/L_{\rm Non}$ with the initial condition given by Eq. (12) for vanishing incoherent optical pumping (i.e., $\Gamma_{31} = 0$). (b) Corresponding contour map for (a).

probe-field intensity $|\Omega_p/U_0|^2$ as a function of τ/τ_0 and $z/L_{\rm Non}$, obtained by using the initial condition (12), with Fig. 3(b) the corresponding contour map of Fig. 3(a). We see that a Peregrine rogue wave appears indeed, which has a sharp peak around $(z,\tau) = (0,0)$ and decays rapidly for large z and τ.

However, one can use a much simpler way to generate (1+1)D Peregrine rogue waves. Figure 3(c) shows the intensity profile $|\Omega_p/U_0|^2$ obtained by using the pure phase engineering [10], with Fig. 3(d) the corresponding contour map of Fig. 3(c). In this way, the initial probe-field amplitude ρ_i is a constant while the initial phase θ_i is chosen from Eq. (12b), which can be produced by using optical phase masks. This is because the initial intensity of the probe field is only weakly modulated [as shown by Eq. (12a)].

We emphasize that the results obtained above is for a nonzero incoherent optical pumping (i.e., $\Gamma_{31} = 9.1 \times 10^4\ {\rm s}^{-1}$), which is crucial for the observation of the rogue waves. Figure 4 shows the result for $\Gamma_{31} = 0$.

We see that in the absence of the incoherent optical pumping the rogue wave suffers a significant attenuation (the maximum intensity of the probe field decreases from $9U_0^2$ to $2U_0^2$) due to the existence of the small residual optical absorption.

Next, we consider the situation $d_{\rm Dis} \ll 1$ and $d_{\rm Dif} = 1$, which can be achieved by taking $L_{\rm Dis} \gg L_{\rm Non}$ and $L_{\rm Dif} = L_{\rm Non}$, i.e., the diffraction and nonlinearity in the system balance each other while the dispersion is negligible, corresponding to the condition $\tau_0 \gg (|\tilde{K}_2|/|\tilde{W}|)^{1/2}U_0^{-1}$ and $R_\perp = [c/(\omega_p|\tilde{W}|)]^{1/2}U_0^{-1}$, respectively. In this case Eq. (8) is reduced to the standard (1+1)D NLS equation

$$i\frac{\partial u}{\partial s} + \frac{1}{2}\frac{\partial^2 u}{\partial \xi^2} + |u|^2 u = 0. \tag{13}$$

As an example for this situation, we take a set of system parameters $\tau_0 = 1.6 \times 10^{-5}$ s and $R_\perp = 0.01$ cm without changing other parameters. The characteristic lengths of the system are given by $L_A \approx 193$ cm, $L_{\rm Dis} = 114$ cm, and $L_{\rm Dif} = L_{\rm Non} \approx 7.2$ cm. We thus have $d_A \approx 0$, $d_{\rm Dis} \approx 0.06$, and $d_{\rm Dif} = 1$. After neglecting the terms proportional to d_A and $d_{\rm Dis}$, Eq. (13) has the first-order Peregrine rogue wave solution with the form $u(s,\xi) = [1 - 4(1 + 2is)/(1 + 4s^2 + 4\xi^2)]e^{is}$, which has the maximum intensity $|u|^2_{\rm max} = 9$, located at $(s,\xi) = (0,0)$. When returning to original variables, we have

$$\Omega_p(z,x) = U_0\left(1 - 4\frac{1 + 2iz/L_{\rm Non}}{1 + 4z^2/L_{\rm Non}^2 + 4x^2/R_\perp^2}\right)e^{iz/L_{\rm Non}}. \tag{14}$$

Thus in this case the rogue wave is a stationary wave packet algebraically decaying in the x and z directions, with the maximum $|\Omega_p|^2_{\rm max} = 9U_0^2$ located at $(x,z) = (0,0)$.

Using the Poynting's vector [36], it is easy to estimate the input power for generating Peregrine rogue waves. For example, the maximum power for the generation of the rogue wave shown in Fig. 3(a) is

$$P_{\rm max} \approx 1.5\,\mu{\rm W}, \tag{15}$$

i.e., very low input power is needed to generate the rogue wave in the present system. Further, the time duration of the input pulse is on the order of microseconds. This is a drastic contrast to conventional media such as glass-based optical fibers, where ps or fs laser pulses are usually needed to reach a very high peak power to bring out the enough nonlinear effect required for the formation of rogue waves [3–6].

B. Ahkmediev and Kuznetsov-Ma breathers in (1+1)D

The standard NLS equation admits also other different types of soliton solutions, in particular Ahkmediev and Kuznetsov-Ma breathers. In the present system, Ahkmediev breathers are localized in the z axis and periodic along the t (or x) axis, whereas Kuznetsov-Ma breathers are localized in the t (or x) axis and periodic along the z axis.

The Ahkmediev breather, after returning to original variables, reads

$$\frac{\Omega_{p,\rm AB}}{U_0} = \frac{(1-4q)\cosh(az/L_{\rm Non}) + \sqrt{2q}\cos(\Omega\tau/\tau_0) + ia\sinh(az/L_{\rm Non})}{\sqrt{2q}\cos(\Omega\tau/\tau_0) - \cosh(az/L_{\rm Non})}e^{iz/L_{\rm Non}}, \tag{16}$$

corresponding to the dispersion-dominant Eq. (9), and

$$\frac{\Omega_{p,\rm AB}}{U_0} = \frac{(1-4q)\cosh(az/L_{\rm Non}) + \sqrt{2q}\cos(\Omega x/R_\perp) + ia\sinh(az/L_{\rm Non})}{\sqrt{2q}\cos(\Omega x/R_\perp) - \cosh(az/L_{\rm Non})}e^{iz/L_{\rm Non}}, \tag{17}$$

corresponding to the diffraction-dominant Eq. (13). Here Ω is a modulation parameter, $q = (1 - \Omega^2/4)/2$, and $a = \sqrt{8q(1-2q)}$. The period of the breather (16) [(17)] along the t (x) axis is $D_t = \pi/\sqrt{1-2q}$ ($D_x = \pi/\sqrt{1-2q}$).

The solutions (16) and (17) are valid only for $q < 1/2$. When $q > 1/2$, we have the Kuznetsov-Ma breather, after returning to original variables, which takes the form

$$\frac{\Omega_{p,\rm KMB}}{U_0} = \frac{(1-4q)\cos(az/L_{\rm Non}) + \sqrt{2q}\cosh(\Omega\tau/\tau_0) - ia\sin(az/L_{\rm Non})}{\sqrt{2q}\cosh(\Omega\tau/\tau_0) - \cos(az/L_{\rm Non})}e^{iz/L_{\rm Non}}, \tag{18}$$

corresponding to the dispersion-dominant Eq. (9), and

$$\frac{\Omega_{p,\mathrm{KMB}}}{U_0} = \frac{(1-4q)\cos(az/L_{\mathrm{Non}}) + \sqrt{2q}\cosh(\Omega x/R_\perp) - ia\sin(az/L_{\mathrm{Non}})}{\sqrt{2q}\cosh(\Omega x/R_\perp) - \cos(az/L_{\mathrm{Non}})} e^{iz/L_{\mathrm{Non}}}, \tag{19}$$

corresponding to the diffraction-dominant Eq. (13). Now one has $q = (1+\Omega^2/4)/2$ and $a = \sqrt{8q(2q-1)}$. The period of the breathers (18) and (19) along the z axis is $D_z = \pi/\sqrt{2q(2q-1)}$. When $q = 1/2$, the Ahkmediev and Kuznetsov-Ma breathers degenerate into the Peregrine rogue waves (10) and (14), respectively.

Shown in Fig. 5(a) is the probe-field intensity $|\Omega_{p,\mathrm{KMB}}/U_0|^2$ for the Kuznetsov-Ma breather as a function of z/L_{Non} and τ/τ_0. The initial condition is taken to be (18) with $\Omega = \sqrt{2}$, $q = 3/4$. In this case, the Kuznetsov-Ma breather oscillates periodically in the z axis, which can be clearly seen in the corresponding contour map illustrated in Fig. 5(b). Figure 5(c) shows $|\Omega_{p,\mathrm{AB}}/U_0|^2$ for the Ahkmediev breather, with the initial condition given by (16) and $\Omega = \sqrt{2}$, $q = 1/4$. We see that in this case the Ahkmediev breather oscillates periodically in the τ axis, as illustrated in the corresponding contour map [i.e., Fig. 5(d)].

The input power for generating the Kuznetsov-Ma breather obtained above can be estimated by calculating the maximum power of the initial condition, which is given by

$$P_{\max} \approx 2.0\,\mu\mathrm{W}. \tag{20}$$

Thus, very low input power is needed for the generation of Ahkmediev and Kuznetsov-Ma breathers in the present system.

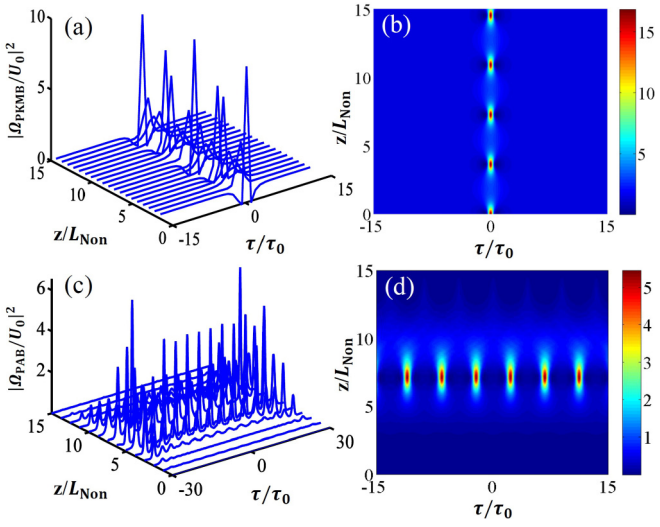

FIG. 5. (a) The probe-field intensity $|\Omega_{p,\mathrm{KMB}}/U_0|^2$ versus τ/τ_0 (with $\tau = t - z/\tilde{V}_g$) and z/L_{Non} for the Kuznetsov-Ma breather. The initial condition is taken to be (18) with $\Omega = \sqrt{2}$ and $q = 3/4$. (b) Corresponding contour map for (a). (c) The probe-field intensity $|\Omega_{p,\mathrm{AB}}/U_0|^2$ versus τ/τ_0 and z/L_{Non} for the Ahkmediev breather. The initial condition is taken to be (16) with $\Omega = \sqrt{2}$ and $q = 1/4$. (d) Corresponding contour map for (c).

V. ACTIVE CONTROL OF THE KUZNETSOV-MA BREATHERS IN (2+1)D

A. Peregrine rogue waves in (2+1)D in the presence of a gradient magnetic field

One of the main advantages of the present system is that it is possible to realize an active control over the probe field by tuning system parameters. One of possibilities is to introduce a gradient magnetic field of the form

$$\mathbf{B}(x) = \hat{\mathbf{z}}B(x) = \hat{\mathbf{z}}B_0 x \tag{21}$$

into the system, where $\hat{\mathbf{z}}$ is the unit vector in the z direction and B_0 characterizes the space gradient of the magnetic field in the x direction, as shown in Fig. 1(b). The gradient magnetic field (21) will result in the Zeeman shift of atomic levels with $\Delta E_{j,\mathrm{Zeeman}}(x) = \mu_B g_F^j m_F^j B(x)$. Here μ_B, g_F^j, and m_F^j are Bohr magneton, gyromagnetic factor, and magnetic quantum number of the level $|j\rangle$, respectively.

The Zeeman shift of atomic levels is equivalent to an external force acting on the atoms, which acts back to the probe field in the system. As a result, an external potential related to the magnetic field will appear in the envelope equation of the probe field. Experimentally, the gradient magnetic field may be realized by using a space-dependent current in coils of wire [38]. Note that such a magnetic field has been used in recent studies on the Stern-Galarch deflection of slow lights [39,40] and ultraslow optical solitons [41,42].

For our aim, the gradient magnetic field is assumed to be weak, i.e., at the order of magnitude of ϵ^3. Then one has $B_0 = \epsilon^3\tilde{B}_0$, and hence $d_{21}^{(2)} = \mu_{21}\tilde{B}_0 x_1$, $d_{31}^{(2)} = \mu_{31}\tilde{B}_0 x_1$, and $d_{32}^{(2)} = \mu_{32}\tilde{B}_0 x_1$, with $\mu_{jl} = \mu_B(g_F^j m_F^j - g_F^l m_F^l)/\hbar$. The nonlinear envelope equation in the presence of the gradient magnetic field (21) can also be derived by the use of the method of multiple scales. But here we are interested in the case in which the probe-field envelope depends on the slow variables x_1, z_2, and t_2 (i.e., the dispersion effect of the system is negligible, valid for the probe pulse with a large time duration). Then we can obtain the following dimensionless envelope equation:

$$i\left(\frac{\partial}{\partial s} + \frac{1}{\lambda}\frac{\partial}{\partial \tau}\right)u + \frac{1}{2}d_{\mathrm{dif}}\frac{\partial^2 u}{\partial \xi^2} + |u|^2 u + p\,\xi u = -i d_A u, \tag{22}$$

where $\tau = t/\tau_0$, $\lambda = V_g\tau_0/L_{\mathrm{Non}}$, and $p = L_{\mathrm{Non}}R_\perp P B_0$ with

$$P = \kappa_{13}\frac{(\omega + d_{21}^{(0)})a_{31}^{(1)}\mu_{31} - \Omega_c a_{21}^{(1)}\mu_{21}}{D} + W', \tag{23}$$

with the expression of W' given in Appendix. Note that p is proportional to the magnetic gradient B_0, which can be used to manipulate the behavior of the probe-field envelope. The expressions of other coefficients are the same with those given below Eq. (8).

As before, by choosing $\Gamma_{31} = 9.1 \times 10^4\ \mathrm{s}^{-1}$, we have $d_A \approx 0$. In addition, we assume $d_{\mathrm{dif}} = 1$, which can be realized

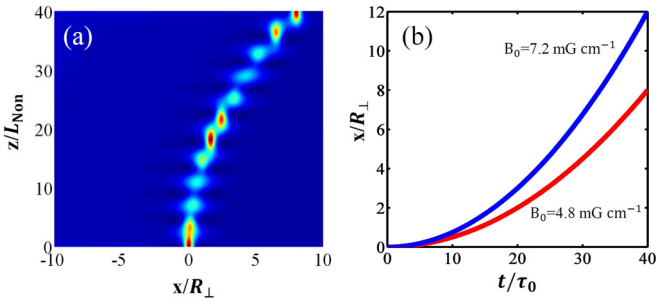

FIG. 6. (a) Trajectory deflection of the Kuznetsov-Ma breather (30) under the action of the gradient magnetic field (21) with $p = 0.01$ (corresponding to $B_0 = 4.8$ mG cm^{-1}). (b) The deflection distance $x/R_\perp$ as a function of time t/τ_0 for $B_0 = 4.8 \times 10^{-3}$ G cm^{-1} [the red (lower) line] and 7.2×10^{-3} G cm^{-1} [the blue (upper) line].

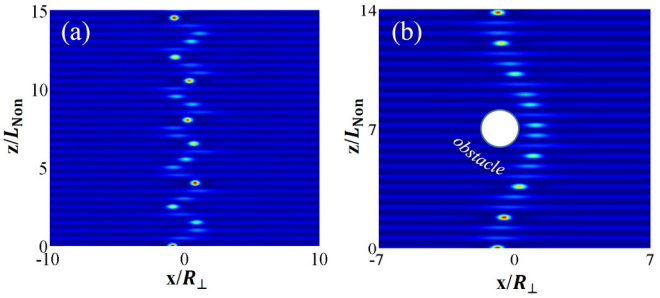

FIG. 7. The traveling trajectory of the Kuznetsov-Ma breather (34) by using the space-time-dependent magnetic field (31) with $\Omega = \sqrt{2}$, $q = 3/4$, and $p = 1$. (a) The case for $\omega_0\tau_0 = 1$; the trajectory is a sinusoidal curve. (b) The case for $\omega_0\tau_0 = 0.1$; the breather can bypass an obstacle (shown by the white solid circle) and recover its input state.

under the condition $L_{\rm Dif} = L_{\rm Non}$. Then Eq. (22) is reduced to

$$i\left(\frac{\partial}{\partial s} + \frac{1}{\lambda}\frac{\partial}{\partial \tau}\right)u + \frac{1}{2}\frac{\partial^2 u}{\partial \xi^2} + |u|^2 u + p\,\xi u = 0. \tag{24}$$

To solve the above equation, we assume [40] $u(s,\tau,\xi) = \psi(s,\tau)\phi(\tau,\xi)$, with

$$\psi(s,\tau) = 2^{1/4} e^{-(s-\lambda\tau)^2/(4\rho^2)} = 2^{1/4} e^{-(z-V_g t)^2/(4\rho^2 L_{\rm Non}^2)}, \tag{25}$$

where ρ is a free real parameter. When writing Eq. (25) the probe-field envelope is assumed to be a Gaussian pulse propagating along the z direction with velocity V_g. In this way, $\phi(\tau,\xi)$ satisfies the following equation:

$$i\frac{1}{\lambda}\frac{\partial \phi}{\partial \tau} + \frac{1}{2}\frac{\partial^2 \phi}{\partial \xi^2} + |\phi|^2\phi + p\,\xi\phi = 0. \tag{26}$$

Then, by making the transformation $\phi = \phi' \exp[i(p\xi' + p^2\tau'^2/3)\tau']$, with $\xi' = \xi - p\tau'^2/2$ and $\tau' = \lambda\tau$, Eq. (26) can be written into the standard NLS equation $i\partial\phi'/\partial\tau' + (1/2)\partial^2\phi'/\partial\xi'^2 + |\phi'|^2\phi' = 0$. Thus, we obtain the Peregrine rogue wave solution of Eq. (24), reading as

$$u(s,\tau,\xi) = 2^{1/4}\left[1 - 4\frac{1 + 2i\lambda\tau}{1 + 4\lambda^2\tau^2 + 4(\xi - p\lambda^2\tau^2/2)^2}\right] \times e^{i\lambda\tau + ip\lambda(\xi - p\lambda^2\tau^2/6)\tau - (s-\lambda\tau)^2/(4\rho^2)}. \tag{27}$$

Returning to original variables, it is given by

$$\Omega_p(z,t,x) = 2^{1/4}U_0\left(1 - 4\frac{1 + 2i\lambda t/\tau_0}{1 + 4\lambda^2 t^2/\tau_0^2 + 4\left[x/R_\perp - p\lambda^2 t^2/(2\tau_0^2)\right]^2}\right) \times e^{i\lambda t/\tau_0 + ip\lambda[x/R_\perp - p\lambda^2 t^2/(6\tau_0^2)]t/\tau_0 - (z/L_{\rm Non} - \lambda t/\tau_0)^2/(4\rho^2)}. \tag{28}$$

We see that the rogue wave (28) is localized in both x and z directions and evolves in time, and hence it is a (2+1)D Peregrine rogue wave. From the rogue wave (28), however, we also observe that the maximum of the rogue wave, locating at $(t,x) = (0,0)$, is independent from the parameter p, which means that one cannot manipulate such maximum of the rogue wave through the gradient magnetic field (21).

B. The manipulation of (2+1)D Kuznetsov-Ma breathers using the gradient magnetic field

Since it is not possible to manipulate the maximum of the (2+1)D Peregrine rogue wave by using the gradient magnetic field, we now turn to consider (2+1)D Ahkmediev and Kuznetsov-Ma breathers. As an example, we study the possibility of an active manipulation for (2+1)D Kuznetsov-Ma breathers. Following the way similar to the last subsection, it is easy to get the Kuznetsov-Ma breather solution of Eq. (24), given by

$$u(s,\tau,\xi) = 2^{1/4}\frac{(1-4q)\cos(a\lambda\tau) + \sqrt{2q}\cosh[\Omega(\xi - p\lambda^2\tau^2/2)] - ia\sin(a\lambda\tau)}{\sqrt{2q}\cosh[\Omega(\xi - p\lambda^2\tau^2/2)] - \cos(a\lambda\tau)} e^{i\lambda\tau + ip\lambda(\xi - p\lambda^2\tau^2/6)\tau - (s-\lambda\tau)^2/(4\rho^2)}, \tag{29}$$

with $q = (1 + \Omega^2/4)/2$ and $a = \sqrt{8q(2q-1)}$. Returning to original variables, it reads

$$\Omega_{p,\rm KMB}(z,t,x) = 2^{1/4}U_0\frac{(1-4q)\cos(a\lambda t/\tau_0) + \sqrt{2q}\cosh\left\{\Omega\left[x/R_\perp - p\lambda^2 t^2/\left(2\tau_0^2\right)\right]\right\} - ia\sin(a\lambda t/\tau_0)}{\sqrt{2q}\cosh\left\{\Omega\left[x/R_\perp - p\lambda^2 t^2/\left(2\tau_0^2\right)\right]\right\} - \cos(a\lambda t/\tau_0)} \times e^{i\lambda t/\tau_0 + ip\lambda[x/R_\perp - p\lambda^2 t^2/(6\tau_0^2)]t/\tau_0 - (z/L_{\rm Non} - \lambda t/\tau_0)^2/(4\rho^2)}. \tag{30}$$

Shown in Fig. 6(a) is the traveling trajectory of the Kuznetsov-Ma breather (30) for $p = 0.01$, which corresponds to $B_0 = 4.8 \times 10^{-3}$ G cm^{-1}. We see that the traveling trajectory is a parabolic type in the presence of the gradient magnetic field.

Figure 6(b) shows the deflection distance $x/R_\perp$ as a function of time t/τ_0 for $B_0 = 4.8 \times 10^{-3}$ G cm^{-1} [the red (lower) line] and 7.2×10^{-3} G cm^{-1} [the blue (upper) line]. We observe that the bending extent of the parabolic trajectory increases as the magnetic field gradient becomes larger.

By using different magnetic fields, one can obtain different shapes of the traveling trajectories for the Kuznetsov-Ma breather. To demonstrate this, we consider a more complicated magnetic field dependent on both space and time, with the form

$$\mathbf{B}(t,x) = \hat{\mathbf{z}}B(t,x) = \hat{\mathbf{z}}B_0 \cos(\omega_0 t)x, \tag{31}$$

where ω_0 characterizes the period of the magnetic field in time. With such a magnetic field and taking into account that $d_{\rm dif} = 1$ and $d_A \approx 0$, Eq. (22) becomes

$$i\left(\frac{\partial}{\partial s} + \frac{1}{\lambda}\frac{\partial}{\partial \tau}\right)u + \frac{1}{2}\frac{\partial^2 u}{\partial \xi^2} + |u|^2 u + p\cos(\omega_0\tau_0\tau)\,\xi u = 0. \tag{32}$$

The Kuznetsov-Ma breather solution of the above equation is given by

$$u(s,\tau) = 2^{1/4}\frac{(1-4q)\cos(a\lambda\tau) + \sqrt{2q}\cosh\left\{\Omega\left[\xi + p\cos(\omega_0\tau_0\lambda\tau)/\left(\omega_0^2\tau_0^2\right)\right]\right\} - ia\sin(a\lambda\tau)}{\sqrt{2q}\cosh\left\{\Omega\left[\xi + p\cos(\omega_0\tau_0\lambda\tau)/\left(\omega_0^2\tau_0^2\right)\right]\right\} - \cos(a\lambda\tau)}$$
$$\times e^{i\lambda\tau + i\Theta - (s-\lambda\tau)^2/(4\rho^2)}, \tag{33}$$

with $\Theta = p[\sin(\omega_0\tau_0\lambda\tau)\xi + p\sin(2\omega_0\tau_0\lambda\tau)/(8\omega_0^2\tau_0^2) - p\lambda\tau/(4\omega_0\tau_0)]/(\omega_0\tau_0)$. Returning to original variables, it reads

$$\Omega_{p,\rm KMB} = 2^{1/4}U_0\frac{(1-4q)\cos(a\lambda t/\tau_0) + \sqrt{2q}\cosh\left\{\Omega\left[x/R_\perp + p\cos(\omega_0\lambda t)/\left(\omega_0^2\tau_0^2\right)\right]\right\} - ia\sin(a\lambda t/\tau_0)}{\sqrt{2q}\cosh\left\{\Omega\left[x/R_\perp + p\cos(\omega_0\lambda t)/\left(\omega_0^2\tau_0^2\right)\right]\right\} - \cos(a\lambda t/\tau_0)}$$
$$\times e^{i\lambda t/\tau_0 + i\Theta - (z/L_{\rm Non} - \lambda t/\tau_0)^2/(4\rho^2)}, \tag{34}$$

with

$$\Theta = \frac{p}{\omega_0\tau_0}\left[\sin(\omega_0\lambda t)\frac{x}{R_\perp} + \frac{p}{8\omega_0^2\tau_0^2}\sin(2\omega_0\lambda t) - \frac{p\lambda t}{4\omega_0\tau_0^2}\right].$$

In Fig. 7(a) we show the trajectory of the Kuznetsov-Ma breather (34) by taking $\Omega = \sqrt{2}$, $q = 3/4$, $\omega_0\tau_0 = 1$, and $p = 1$ (corresponding to $B_0 = 0.48$ G cm^{-1}). We see that in the presence of the space-time-dependent magnetic field (31), the traveling trajectory of the Kuznetsov-Ma breather follows a sinusoidal curve. Shown in Fig. 7(b) is the trajectory for $p = 1$ and $\omega_0\tau_0 = 0.1$. We observe that in this case the breather can bypass an obstacle (indicated by the white solid circle) and recover its initial input state. The manipulations of Kuznetsov-Ma breathers (30) and (34) by using external magnetic fields shown above are not only interesting in theory but also promising in applications on the active control of these nonlinear excitations.

VI. SUMMARY

To sum up, in this work we have suggested a scheme to demonstrate the existence of optical Peregrine rogue waves and Akhmediev and Kuznetsov-Ma breathers and realized their active control via EIT in a cold, three-level atomic system with a Λ-type level configuration. Based on the EIT with an incoherent optical pumping, which is used for canceling the optical absorption, we have shown that (1+1)D optical Peregrine rogue waves, Akhmediev breathers, and Kuznetsov-Ma breathers can be created by using very low light intensity. In addition, we have demonstrated that the Akhmediev and Kuznetsov-Ma breathers in (2+1)D obtained can be actively manipulated by using an external magnetic field. As a result, these breathers may display trajectory deflections and bypass obstacles during propagation. The results obtained may have potential applications in optical information processing and transmission.

ACKNOWLEDGMENTS

J.Y.L. was supported by the East China Normal University under Grant No. YJSKC2015-17. C.H. was supported by the National Natural Science Foundation of China under Grant No. 11475063, and G.X.H. was supported by the National Natural Science Foundation of China under Grants No. 11174080 and No. 11474099.

APPENDIX: EXPLICIT EXPRESSIONS OF SOME COEFFICIENTS APPEARING IN SEC. III

The expressions of $a_{31}^{(1)}$ and $a_{21}^{(1)}$ in the first-order solution of the MB equations are given by

$$a_{31}^{(1)} = \frac{\Omega_c\sigma_{32}^{(0)*} + \left(\omega + d_{21}^{(0)}\right)\left(\sigma_{11}^{(0)} - \sigma_{33}^{(0)}\right)}{D(\omega)}, \tag{A1a}$$

$$0a_{21}^{(1)} = -\frac{\Omega_c^*\left(\sigma_{11}^{(0)} - \sigma_{33}^{(0)}\right) + \left(\omega + d_{31}^{(0)}\right)\sigma_{32}^{(0)*}}{D(\omega)}, \tag{A1b}$$

with $D(\omega) = |\Omega_c|^2 - (\omega + d_{21}^{(0)})(\omega + d_{31}^{(0)})$.

The expressions of $a_{31}^{(2)}$, $a_{21}^{(2)}$, $a_{11}^{(2)}$, $a_{22}^{(2)}$, and $a_{32}^{(2)}$ in the second-order solution of the MB equations are given by

$$a_{31}^{(2)} = \frac{i}{\kappa_{13}}\left(\frac{1}{V_g} - \frac{1}{c}\right), \tag{A2}$$

$$a_{21}^{(2)} = -\frac{i}{\Omega_c}\left[a_{31}^{(1)} + \frac{\left(\omega + d_{31}^{(0)}\right)}{\kappa_{13}}\left(\frac{1}{V_g} - \frac{1}{c}\right)\right], \tag{A3}$$

$$a_{11}^{(2)} = \frac{(\Gamma_{23} - 2i|\Omega_c|^2 X)\left(a_{31}^{(1)*} - a_{31}^{(1)}\right) + \Gamma_{13}\Omega_c a_{21}^{(1)}/\left(\omega + d_{32}^{(0)*}\right) - \Gamma_{13}\Omega_c^* a_{21}^{(1)*}/\left(\omega + d_{32}^{(0)}\right)}{i\Gamma_{31}\Gamma_{23} + |\Omega_c|^2 X(2\Gamma_{31} + \Gamma_{13})}, \tag{A4}$$

$$a_{22}^{(2)} = \frac{a_{31}^{(1)*} - a_{31}^{(1)}}{i\Gamma_{13}} - \frac{\Gamma_{31} + \Gamma_{13}}{\Gamma_{13}} a_{11}^{(2)}, \tag{A5}$$

$$a_{32}^{(2)} = -\frac{a_{21}^{(1)*}}{\left(\omega + d_{32}^{(0)}\right)} - \frac{2\Omega_c\left(a_{31}^{(1)*} - a_{31}^{(1)}\right)}{i\Gamma_{13}\left(\omega + d_{32}^{(0)}\right)} + \frac{\Omega_c(2\Gamma_{31} + \Gamma_{13})}{\Gamma_{13}\left(\omega + d_{32}^{(0)}\right)} a_{11}^{(2)}. \tag{A6}$$

The expression of W' in Eq. (23) reads

$$W' = \kappa_{13}\frac{\Omega_c A^* + \left(\omega + d_{21}^{(0)}\right)(2B + C)}{D}, \tag{A7}$$

with

$$A = -\frac{d_{32}^{(2)}\sigma_{32}^{(0)} + \Omega_c(B + 2C)}{\left(\omega + d_{32}^{(0)}\right)}, \tag{A8}$$

$$B = \frac{\Gamma_{13}\Omega_c/\left(\omega + d_{32}^{(0)*}\right)d_{32}^{(2)*}\sigma_{32}^{(0)*} - \Gamma_{13}\Omega_c^*/\left(\omega + d_{32}^{(0)}\right)d_{32}^{(2)}\sigma_{32}^{(0)}}{i\Gamma_{31}\Gamma_{23} + |\Omega_c|^2 X(2\Gamma_{31} + \Gamma_{13})}, \tag{A9}$$

$$C = -\frac{\Gamma_{31}\Gamma_{13}}{\Gamma_{13}} a_{11}^{(22)}. \tag{A10}$$

[1] E. Pelinovsky and C. Kharif, *Extreme Ocean Waves* (Springer, Berlin, 2008).

[2] A. R. Osborne, *Nonlinear Ocean Waves and the Inverse Scattering Transform* (Elsevier, New York, 2010).

[3] D. R. Solli, C. Ropers, P. Koonath, and B. Jalali, Optical rogue waves, Nature (London) **450**, 1054 (2007).

[4] A. Montina, U. Bortolozzo, S. Residori, and F. T. Arecchi, Non-Gaussian Statistics and Extreme Waves in a Nonlinear Optical Cavity, Phys. Rev. Lett. **103**, 173901 (2009).

[5] B. Kibler, J. Fatome, C. Finot, G. Millot, F. Dias, G. Genty, N. Akhmediev, and J. M. Dudley, The Peregrine soliton in nonlinear fibre optics, Nat. Phys. **6**, 790 (2010).

[6] A. Zaviyalov, O. Egorov, R. Iliew, and F. Lederer, Rogue waves in mode-locked fiber lasers, Phys. Rev. A **85**, 013828 (2012).

[7] A. Chabchoub, N. P. Hoffmann, and N. Akhmediev, Rogue Wave Observation in a Water Wave Tank, Phys. Rev. Lett. **106**, 204502 (2011).

[8] H. Bailung, S. K. Sharma, and Y. Nakamura, Observation of Peregrine Solitons in a Multicomponent Plasma with Negative Ions, Phys. Rev. Lett. **107**, 255005 (2011).

[9] S. Birkholz, E. T. J. Nibbering, C. Bree, S. Skupin, A. Demircan, G. Genty, and G. Steinmeyer, Spatiotemporal Rogue Events in Optical Multiple Filamentation, Phys. Rev. Lett. **111**, 243903 (2013).

[10] Yu. V. Bludov, V. V. Konotop, and N. Akhmediev, Matter rogue waves, Phys. Rev. A **80**, 033610 (2009).

[11] A. Coillet, J. Dudley, G. Genty, L. Larger, and Y. K. Chembo, Optical rogue waves in whispering-gallery-mode resonators, Phys. Rev. A **89**, 013835 (2014).

[12] D. Pierangeli, F. Di Mei, C. Conti, A. J. Agranat, and E. DelRe, Spatial Rogue Waves in Photorefractive Ferroelectrics, Phys. Rev. Lett. **115**, 093901 (2015).

[13] N. Akhmediev, A. Ankiewicz, and J. M. Soto-Crespo, Rogue waves and rational solutions of the nonlinear Schrodinger equation, Phys. Rev. E **80**, 026601 (2009).

[14] W.-P. Zhong, M. R. Belic, and T. Huang, Rogue wave solutions to the generalized nonlinear Schrödinger equation with variable coefficients, Phys. Rev. E **87**, 065201 (2013).

[15] H. N. Chan, K. W. Chow, D. J. Kedziora, R. H. J. Grimshaw, and E. Ding, Rogue wave modes for a derivative nonlinear Schrodinger model, Phys. Rev. E **89**, 032914 (2014).

[16] A. Ankiewicz, J. M. Soto-Crespo, and N. Akhmediev, Rogue waves and rational solutions of the Hirota equation, Phys. Rev. E **81**, 046602 (2010).

[17] Y. Tao and J. He, Multisolitons, breathers, and rogue waves for the Hirota equation generated by the Darboux transformation, Phys. Rev. E **85**, 026601 (2012).

[18] S. Chen and L. Song, Rogue waves in coupled Hirota systems, Phys. Rev. E **87**, 032910 (2013).

[19] Y. Ohta and J. Yang, Rogue waves in the Davey-Stewartson I equation, Phys. Rev. E **86**, 036604 (2012).

[20] N. Akhmediev, J. M. Soto-Crespo, and A. Ankiewicz, Extreme waves that appear from nowhere: On the nature of rogue waves, Phys. Lett. A **373**, 2137 (2009).

[21] D. H. Peregrine, Water waves, nonlinear Schrödinger equations and their solutions, J. Aust. Math. Soc. Ser. B **25**, 16 (1983).

[22] Y.-C. Ma, The perturbed plane-wave solution of the cubic Schrödinger equation, Stud. Appl. Math. **60**, 43 (1979).

[23] N. Akhmediev, V. Eleonskii, and N. Kulagin, Exact first-order solutions of the nonlinear Schrödinger equation, Theor. Math. Phys. **72**, 809 (1987).

[24] M. Erkintalo, K. Hammani, B. Kibler, C. Finot, N. Akhmediev, J. M. Dudley, and G. Genty, Higher-Order Modulation Instability in Nonlinear Fiber Optics, Phys. Rev. Lett. **107**, 253901 (2011).

[25] Z. Yan, V. V. Konotop, and N. Akhmediev, Three-dimensional rogue waves in nonstationary parabolic potentials, Phys. Rev. E **82**, 036610 (2010).

[26] F. Baronio, A. Degasperis, M. Conforti, and S. Wabnitz, Solutions of the Vector Nonlinear Schrödinger Equations: Evidence for Deterministic Rogue Waves, Phys. Rev. Lett. **109**, 044102 (2012).

[27] C. Bonatto, M. Feyereisen, S. Barland, M. Giudici, C. Masoller, J. R. R. Leite, and J. R. Tredicce, Deterministic Optical Rogue Waves, Phys. Rev. Lett. **107**, 053901 (2011).

[28] J. M. Dudley, F. Dias, M. Erkintalo, and G. Genty, Instabilities, breathers and rogue waves in optics, Nat. Photon. **8**, 755 (2014).

[29] D. R. Solli, C. Ropers, and B. Jalali, Active Control of Rogue Waves for Stimulated Supercontinuum Generation, Phys. Rev. Lett. **101**, 233902 (2008).

[30] Y. Zhang, M. R. Belić, H. Zheng, H. Chen, C. Li, J. Song, and Y. Zhang, Nonlinear Talbot effect of rogue waves, Phys. Rev. E **89**, 032902 (2014).

[31] M. Fleischhauer, A. Imamoglu, and J. P. Marangos, Electromagnetically induced transparency: Optics in coherent media, Rev. Mod. Phys. **77**, 633 (2005).

[32] For neglecting the Doppler effect, it requires that the Doppler width $W_D = k_p\sqrt{2k_BT/M}$ (here T is the temperature and M is the atomic mass of rubidium) should be much less than γ_{31}, i.e., $W_D \ll \gamma_{31}$ [see L. Liang and G. Huang, Linear and nonlinear light propagations in a Doppler-broadened medium via electromagnetically induced transparency, Phys. Rev. A **82**, 023809 (2010)]; with the parameters given in the last paragraph of Sec. II, it results in the condition $T \ll 0.1$ K.

[33] R. W. Boyd, *Nonlinear Optics*, 3rd ed. (Academic, San Diego, CA, 2008).

[34] G. Huang, L. Deng and M. G. Payne, Dynamics of ultraslow optical solitons in a cold three-state atomic system, Phys. Rev. E **72**, 016617 (2005).

[35] D. Steck, ^{85}Rb D Line Data, http://steck.us/alkalidata.

[36] A. C. Newell and J. V. Moloney, *Nonlinear Optics* (Addison-Wesley, Redwood City, 1992).

[37] The frequency and wave number of the probe field are given by $\omega_p + \omega$ and $k_p + K(\omega)$, respectively. Thus $\omega = 0$ corresponds to the center frequency of the probe field.

[38] J. D. Jackson, *Classical Electrodynamics*, 3rd ed. (Wiley, New York, 1998).

[39] L. Karpa and M. Weitz, A Stern-Gerlach experiment for slow light, Nat. Phys. **2**, 332 (2006).

[40] Y. Guo, L. Zhou, L. Kuang, and C. P. Sun, Magneto-optical Stern-Gerlach effect in an atomic ensemble, Phys. Rev. A **78**, 013833 (2008).

[41] C. Hang and G. Huang, Stern-Gerlach effect of weak-light ultraslow vector solitons, Phys. Rev. A **86**, 043809 (2012).

[42] Z. Chen and G. Huang, Stern-Gerlach effect of multi-component ultraslow optical solitons via electromagnetically induced transparency, J. Opt. Soc. Am. B **30**, 2248 (2013).